ANNUAL REVIEWS

Annual Review of Physical Chemistry

Control of Chemical Reaction Pathways by Light–Matter Coupling

Dinumol Devasia,[1] Ankita Das,[1] Varun Mohan,[2] and Prashant K. Jain[1,3]

[1]Department of Chemistry, University of Illinois at Urbana-Champaign, Urbana, Illinois 61801, USA; email: jain@illinois.edu

[2]Department of Materials Science and Engineering, University of Illinois at Urbana-Champaign, Urbana, Illinois 61801, USA

[3]Department of Physics, Materials Research Lab, and Beckman Institute for Advanced Science and Technology, University of Illinois at Urbana-Champaign, Urbana, Illinois 61801, USA

Annu. Rev. Phys. Chem. 2021. 72:423–43

First published as a Review in Advance on January 22, 2021

The *Annual Review of Physical Chemistry* is online at physchem.annualreviews.org

https://doi.org/10.1146/annurev-physchem-090519-045502

Keywords

heterogeneous catalysis, plasmons, localized surface plasmon resonance, LSPR, hot electrons, activation, electron transfer

Abstract

Because plasmonic metal nanostructures combine strong light absorption with catalytically active surfaces, they have become platforms for the light-assisted catalysis of chemical reactions. The enhancement of reaction rates by plasmonic excitation has been extensively discussed. This review focuses on a less discussed aspect: the induction of new reaction pathways by light excitation. Through commentary on seminal reports, we describe the principles behind the optical modulation of chemical reactivity and selectivity on plasmonic metal nanostructures. Central to these phenomena are excited charge carriers generated by plasmonic excitation, which modify the energy landscape available to surface reactive species and unlock pathways not conventionally available in thermal catalysis. Photogenerated carriers can trigger bond dissociation or desorption in an adsorbate-selective manner, drive charge transfer and multielectron redox reactions, and generate radical intermediates. Through one or more of these mechanisms, a specific pathway becomes favored under light. By improved control over these mechanisms, light-assisted catalysis can be transformational for chemical synthesis and energy conversion.

1. INTRODUCTION

Heterogeneous catalysis based on transition metals is a trillion-dollar industry in which chemicals are often manufactured under energy-intensive conditions of elevated temperatures and pressures (1). Replacing these demanding conditions with alternative means of chemical activation such as light excitation would be desirable. Catalysis assisted by light excitation is attractive because photoenhancement can allow meaningfully high reaction rates to be achieved at lower operating temperatures and/or ambient conditions. With the strategic use of light, not only can energy demands for heating be lowered, but also the stability of the catalyst, which otherwise deteriorates under higher temperatures or harsher conditions, can be maintained (2–11). Motivated by these opportunities, the use of light for inducing, enhancing, and tuning the activities of chemical catalysts has become a staple in academic and industrial research.

Using light instead of heat to drive catalytic reactions is rooted in the principles of molecular photochemistry. A catalyst reduces the activation barrier of a reaction, often by the adsorption or complexation of one or more reactants with the catalyst surface. In so-called dark thermal catalysis, a high-temperature bath facilitates overcoming the activation energy barrier (12, 13). The catalyst–reactant system proceeds along the ground electronic potential energy surface (PES) to form the products. However, under light excitation, the catalyst–reactant complex can be elevated to an excited electronic state, provided the complex can absorb light or a photosensitizer is present. The reaction then progresses by evolution of the catalyst–reactant complex along the electronically excited PES. This excited-state pathway offers an effectively lower activation barrier and an accelerated reaction rate compared to those of the dark pathway. This phenomenon is referred to as light-assisted catalysis or photocatalysis. In some cases, in addition to reaction rate enhancement, the electronic excitation provides a thermodynamic potential for driving a reaction that is otherwise endergonic ($\Delta G > 0$) and nonspontaneous in the dark. Such a reaction is photosynthetic (14). There is yet another salient attribute of light-assisted catalysis. Whereas the use of heat is nonselective in its enhancement of reaction rates, light excitation can be used to access specific PESs and facilitate specific reaction pathways. Furthermore, the photoinduced pathway may be tunable by the variation of light excitation attributes such as photon energy and intensity.

The coupling of light excitation to a chemical reaction pathway is accomplished by the use of a catalyst or a sensitizer with light absorption in the ultraviolet (UV)–visible–near infrared region (15). While molecular absorbers form an entire class of their own, a growing number of examples of light-assisted catalysis employ plasmonic metal nanoparticles (NPs) or hybrids of plasmonic metal NPs and semiconductors (16). These nanostructures are platforms for strong light–matter coupling. In addition, because they possess tunable light absorption, high specific surface areas, and surface chemistry that can be engineered, plasmonic nanostructures have been employed for the light-assisted catalysis of energy-relevant and industrial reactions, such as water splitting (17, 18), CO_2 fixation (19–22), methane reforming (23), alkene epoxidation (2), and hydrogen dissociation (8).

Unlike molecular photochemistry, for which a paradigm is well established, photoassisted catalysis on light-absorbing nanostructures does not have a unified physicochemical model. Therefore, we review here, with the aid of key examples, the conceptual principles and putative mechanisms by which strong light–matter interactions are exploited in heterogeneous catalysis. The discussion is centered on the photophysics and dynamics of the carriers thought to be responsible for the modulation of catalytic behavior. We hope that this collective knowledge will lead to the design of strategies for the light-mediated control of the rate, selectivity, and chemical pathway of a reaction. With the use of light-mediated control, catalysts can be repurposed rather than synthesized de novo for chemical processes of interest.

2. FUNCTIONAL ATTRIBUTES OF PLASMONIC METAL NANOPARTICLES FOR LIGHT-ASSISTED CATALYSIS

In recent years, metal NPs (24–27), particularly those of the coinage metals Au, Ag, and Cu, have been found to exhibit light-assisted catalysis. This photoactivity originates from the ability of these metals to adsorb small molecules coupled with their strong interaction with light. An electromagnetic field of a specific band of frequencies induces a resonant collective oscillation of the free electrons of the metal, which is known as a plasmon. In an NP, this oscillation is bounded by the surface of the NP and is termed a localized surface plasmon resonance (LSPR). For the coinage metals, the resonance frequencies typically lie in the visible range of the spectrum. Due to this resonant interaction, the visible-light absorption cross sections of these NPs often exceed their geometrical cross sections (28) at frequencies coincident with the LSPR. Plasmonic NPs function effectively as optical nanoantennas that concentrate the light of resonant frequencies by focusing it down to subdiffraction length scales (29–31). Intense electric fields are sustained on the NP surface under resonant photoexcitation (32–39). While these intense fields have been suggested to influence chemical activity, here we focus on the chemical action of excited charge carriers generated by LSPR excitation. A detailed discussion of the mechanisms and models deduced from experimental studies follows.

3. PHOTOGENERATED CARRIER DYNAMICS RELEVANT TO LIGHT-ASSISTED CATALYSIS

Compared to electronic excitations in molecular chromophores, LSPRs excited in a metal NP are short-lived. An LSPR undergoes dephasing within 1–10 fs, followed by either radiative damping, which involves the emission of photons, or nonradiative damping (40–42). In NPs much smaller than the wavelength of light, the contribution of the radiative pathway is minor (43, 44). Moreover, it is the nonradiative pathway that is relevant for light-assisted catalysis. The excited carriers, that is, electron–hole pairs, formed by plasmon dephasing constitute a nonthermal distribution. By electron–electron scattering processes on the 100-fs timescale, this distribution thermalizes to form a hot Fermi-Dirac distribution. The electronic temperature of this distribution is higher than the lattice temperature. The hot Fermi-Dirac distribution and the colder lattice of the NP undergo mutual thermal equilibration by electron–phonon scattering on the timescale of 100 fs to 1 ps. This process heats up the NP lattice. Eventually, the heat is transferred into the surrounding medium by phonon–phonon scattering on the 100-ps timescale (30, 45). Thus, there is only a small window of time of a few femtoseconds to 1 ps between plasmon excitation and thermal dissipation for energetic charge carriers to be harvested from the NP for a chemical reaction (19, 29, 46–51). This is the core challenge in the deployment of plasmonic NPs for light-driven catalysis (52–55). The availability of adsorbates or electron acceptors at the metal NP surface can help meet this challenge. With chemisorbed molecules that are electronically coupled to the metal, excited electrons—from states above the Fermi level—can be transferred on subpicosecond timescales to the adsorbate, thereby triggering chemical reactions (50). Alternatively, electrons can be injected by an adsorbate into empty states in the metal NP below the Fermi level. The faster the carrier transfer is, the more efficiently—in photon utilization terms—chemical activity can be induced by photoexcitation of the plasmonic NP (52).

The metal NP-to-adsorbate charge transfer can be irreversible; the mechanism for this type of transfer is discussed in Section 4.3. However, in general, the charge transfer is reversible. Excited electrons transfer to the unoccupied antibonding states of the metal–adsorbate complex, forming a transient negative ion (TNI) (56) as a result. The TNI is short-lived, but during its lifetime, nuclear motion can take place on the excited PES, triggering either the formation, dissociation,

or weakening of molecular bonds in the metal–adsorbate complex (32). Following the lifetime of the TNI, the electron relaxes either inelastically by scattering with the colder metal electron sea or elastically by back-electron transfer to resonant metallic electronic states (57). The latter process leaves the metal–adsorbate complex in a vibrationally excited state that is susceptible to a chemical transformation such as bond dissociation. If multiple such excitation–deexcitation cycles occur within the relaxation time of metal–adsorbate vibrations, the accumulated vibrational energy of the complex can become large enough to trigger bond dissociation. The process is analogous to the phenomenon in ultrafast surface photochemistry known as desorption induced by electronic transitions (58, 59), in which a single excitation is sufficient for triggering the dissociation, or desorption induced by multiple electronic transitions (60), in which multiple excitations are involved.

The transient interfacial electron transfer from a metal NP to an adsorbate can occur by either indirect or direct transfer (29, 61, 62). In the indirect transfer mechanism, excited carriers are first formed in the metal NP by LSPR damping. Subsequent to this, the carriers with sufficient energy are transferred to an unoccupied molecular orbital (MO) of the adsorbate, forming the TNI (52, 63). In contrast, in the direct transfer mechanism, coherent with the LSPR damping, electrons are excited from occupied to unoccupied orbitals of the metal–adsorbate complex (24, 62, 64–68), forming the TNI.

If the transfer of electrons is slower than the process of thermal dissipation, electron-mediated chemistry is not feasible (58, 60). Instead, photoexcitation results in the heating of the NP and the surrounding medium. The elevated temperature can more easily overcome activation barriers and enhance reaction rates, as described by the Arrhenius law. However, there is no charge transfer (12, 13). The reaction dynamics is dictated by the ground-state PES. In such a case, the reaction mechanism, the products, and their distribution are all similar to those of a thermally catalyzed process conducted in the dark at the elevated temperature. In contrast, the action of photogenerated carriers triggers reaction pathways that depart from the purely thermal process. As a consequence, the products and their distributions can differ from those of the thermal pathway. Thus, the competition between the thermalization of hot carriers and interfacial electron transfer dictates whether unique plasmon-activated chemistry is observed.

Specific bonds in the adsorbate may be targeted by plasmonic excitation. Especially when the direct mechanism of transfer is operative, the excitation photon energy dictates which acceptor states in the metal–adsorbate complex are populated. Such state selection in turn influences which bonds are selectively activated. The control of reaction selectivity through the choice of the excitation photon energy is made easier by the tunability of plasmonic NPs (69–72). By variation of the size, shape, composition, or the medium of metal NPs (37, 43, 73–75), the LSPR frequency can be tuned across the entire visible spectrum. Thus, through appropriate design of the metal nanostructure, the absorption cross section is ensured to be large enough at the excitation photon energy chosen to trigger a particular reaction outcome.

4. MECHANISMS OF LIGHT-ASSISTED CATALYSIS ON PLASMONIC NANOPARTICLES

In the following sections, we describe, using seminal examples, how the photoexcitation of plasmonic NPs and the ensuing carrier dynamics allow the targeting of specific reaction pathways.

4.1. Photodissociation of Strong Covalent Bonds

Small molecules such as H_2, O_2, and SO_x have large bond dissociation enthalpies and large highest-occupied MO (HOMO)–lowest-unoccupied MO (LUMO) gaps that are accessible only

by UV light (2, 4, 7, 8, 76–78). Visible-light-induced photodissociation of these molecules does not occur under normal circumstances. However, visible-light excitation of plasmonic NPs has been found to trigger the dissociation of adsorbed molecules (2, 7, 8, 79–81). This phenomenon is attributed to the action of hot electrons formed by plasmonic excitation (**Figure 1**).

4.1.1. Indirect hot electron transfer. Some of the observed photodissociation reactions, described in this subsection, are thought to be induced by the transfer of electrons from the NP to the adsorbate by the indirect mechanism.

4.1.1.1. H_2 dissociation. The dissociation of H_2 was observed to occur on photocatalysts consisting of Au NPs supported on metal oxides, either TiO_2 or SiO_2, under visible-light irradiation (7, 8). The dissociation reaction proceeded at significant rates even down to room temperature. The rate of H_2 dissociation was measured across a range of light intensities and wavelengths at a fixed temperature of 373 K. The rate was found to scale linearly with the light intensity. The wavelength dependence of the rate tracked with the wavelength dependence of the calculated absorption cross section. These trends confirm that light absorption by the Au NPs is responsible for the observed H_2 dissociation. The rate under 2.4 W/cm^2 of white-light illumination was sixfold higher than that under dark conditions (**Figure 1*b***). This enhancement was attributed to the chemical action of hot electrons.

Based on photoreaction studies supported by density functional theory (DFT) simulations, Halas and coworkers (8) proposed a model for the observed photodissociation. H_2 weakly physisorbs to the surface of Au. Interaction with the Au surface involves an energetic downshift of the bonding (B) and antibonding (AB) orbitals of H_2. Due to a shift to energies below the Fermi level of Au along with a broadening resulting from hybridization with the *s*-band states of Au, the AB $1\sigma_u^*$ orbital may become partially occupied, weakening the H–H bond even in the dark. Visible-light excitation of LSPRs in the Au NPs creates a distribution of hot electrons; electrons in the high-energy tail of this distribution can transfer to the AB orbital of adsorbed H_2 and create a TNI, $H_2^{\delta-}$ (**Figure 1*a***), with an elongated H–H bond. Eventually, the electron returns to the Au NP, and adsorbed H_2 returns to its ground-state PES in a vibrationally excited state with a stretched, that is, an activated H–H bond. From this activated state, it is relatively easy to migrate to the dissociated state.

4.1.1.2. O_2 dissociation. In a seminal study, Linic and coworkers (2) observed the visible-light-induced dissociation of O_2 on an Ag NP surface. A mechanism similar to the one described in Section 4.1.1.1 is thought to be responsible. Hot electrons generated by LSPR excitation transfer from Ag to the unoccupied electronic states ($2\pi^*$ AB orbital) of adsorbed O_2, generating a TNI, O_2^-. The TNI then relaxes, depositing vibrational energy in the O–O bond and triggering bond dissociation. Linic and coworkers (2) found that the O_{ads} atoms formed by dissociation can be used to conduct oxidation reactions, such as the oxidation of ethylene to ethylene oxide, at lower temperatures and pressures than those employed in conventional thermally catalyzed oxidation. The rate of ethylene oxidation achieved by the visible-light excitation of Ag NPs was found to be greater than that in the dark. Further mechanistic study of visible-light-mediated ethylene oxidation has been conducted by Jain and coworkers (82).

4.1.2. Direct hot electron transfer. The direct electron-transfer mechanism becomes relevant in metal–adsorbate systems with strong hybridization between the adsorbate orbitals and metal surface states. This is typically the case in chemisorption. The metal–adsorbate electronic admixture has HOMO-derived MOs of predominantly metal character and LUMO-derived MOs that

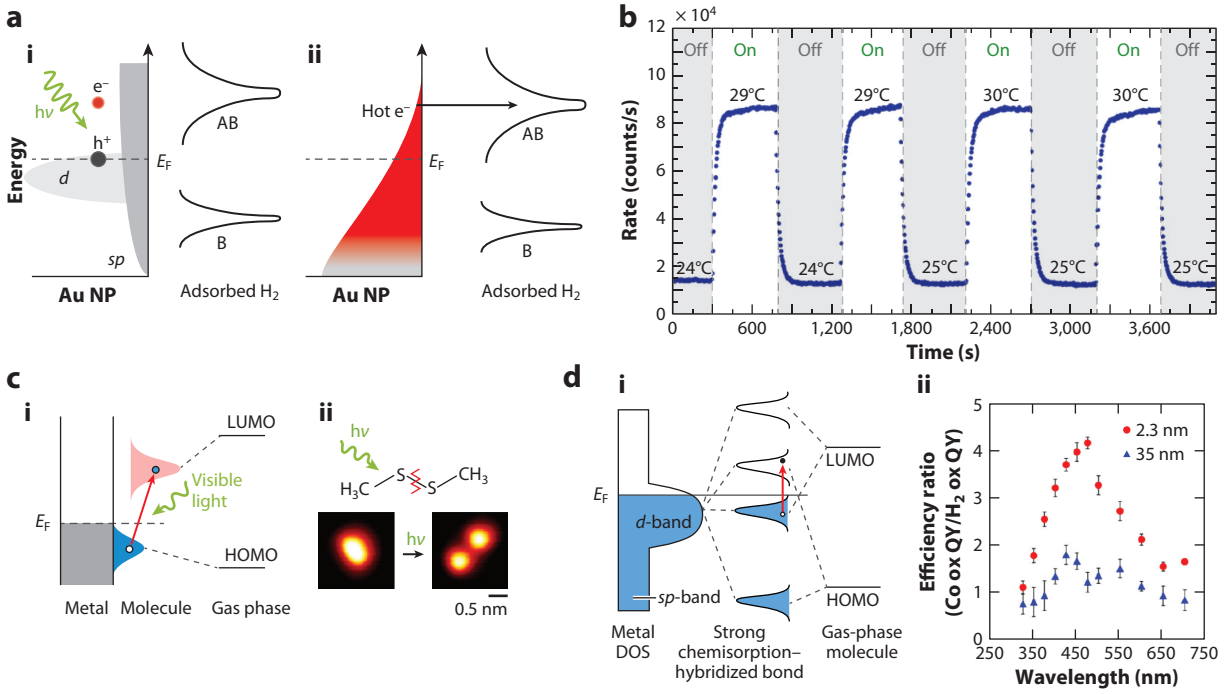

Figure 1

Photodissociation of bonds in adsorbates on plasmonic metal NPs. Panels *a* and *b* show indirect electron transfer, while panels *c* and *d* show direct electron transfer. (*a*) Schematic illustrations showing the processes involved in the visible-light (hν)-excitation-induced dissociation of H_2 on Au NPs supported on TiO_2. (*i*) An LSPR excited in the Au NP undergoes damping to form an excited electron–hole (e^-–h^+) pair. B and AB denote the electronic states of H_2, which is weakly physisorbed onto the Au NP surface. The density of states of the *d*-band is shown by light gray shading; the density of states of the *sp*-band is shown by darker gray shading. (*ii*) The excited electrons thermalize to a hot Fermi-Dirac distribution; electrons in the high-energy tail possess adequate energy to populate AB states in the adsorbed H_2, generating the TNI $H_2^{\delta-}$ with an extended H–H bond. The TNI relaxes to the ground electronic state via back-electron transfer to the Au NP. The vibrationally excited H_2 formed as a result easily dissociates. The red-shaded region identifies filled electronic states. (*b*) Graph showing the rate of H_2 dissociation on TiO_2-supported Au NPs with 2.4 W/cm^2 laser excitation (*green*, *on*) and without laser excitation (*gray*, *off*). Laser excitation causes an increase in the H_2 dissociation rate and an elevation of the photocatalyst temperature from 24°C to 29°C. Panels *a* and *b* adapted with permission from Reference 8; copyright 2013 American Chemical Society. (*c*) Schematic of the mechanism of visible-light-induced photodissociation of $(CH_3S)_2$. (*i*) Visible light drives a direct electronic transition (*red arrow*) between the hybridized electronic states, specifically the HOMO- and LUMO-derived states, of the metal–$(CH_3S)_2$ complex, leading to S–S bond scission. E_F indicates the Fermi level of the metal. (*ii*) Scanning tunneling microscopy images showing the photodissociation of the S–S bond with 532-nm light excitation. Panel *c* adapted with permission from Reference 78; copyright 2017 American Chemical Society. (*d*) Schematic showing visible-light-induced desorption of CO from a Pt surface. (*i*) Surface *sp*- and *d*-states of Pt and molecular orbitals of CO undergo hybridization. E_F indicates the Fermi level of the metal, and filled states are shaded in blue. A direct electronic transition (*red arrow*) between the hybridized orbitals is possible with the use of light of a wavelength (i.e., 470 nm) resonant with the gap between the HOMO- and LUMO-derived orbitals. This results in selective photoactivation of the Pt–CO bond and desorption. (*ii*) Excitation of 2.3-nm Pt NPs supported on α-Al_2O_3 by 470-nm light results in adsorbed CO being oxidized more efficiently than H_2. This is depicted by the wavelength dependence of the efficiency ratio, that is, the ratio of the QY of CO ox to that of H_2 ox, which peaks at ~470 nm, the wavelength resonant with the gap. The preferential CO ox seen for 2.3-nm Pt NPs is not significant for 35-nm Pt NPs. Panel *d* adapted with permission from Reference 83; copyright 2014 American Chemical Society. Abbreviations: AB, antibonding; B, bonding; CO ox, CO oxidation; DOS, density of states; H_2 ox, H_2 oxidation; HOMO, highest-occupied molecular orbital; LSPR, localized surface plasmon resonance; LUMO, lowest-unoccupied molecular orbital; NP, nanoparticle; QY, quantum yield; TNI, transient negative ion.

are mostly molecular in character. By employing the light of a photon energy matching the energy gap of the electronic admixture (49, 62, 65, 67, 78, 83), hot electrons can be directly excited from the metal NP to the adsorbate, thereby triggering chemical transformations of the adsorbate. The photon energy required to achieve such a direct electron transfer and the electron-transfer efficiency vary from one adsorbate to another depending on the extent of orbital hybridization. The direct electron-transfer mechanism is thought to be operative in photodissociation on plasmonic NPs, one example of which is described next.

Using scanning tunneling microscopy, Kazuma et al. (61, 78) demonstrated visible-light-induced S–S bond dissociation in dimethyl disulfide, $(CH_3S)_2$, on Cu(111) and Ag(111). DFT calculations indicated that when the states of the metal (Cu and Ag) strongly hybridize with the orbitals of $(CH_3S)_2$, the gap between HOMO- and LUMO-derived MOs reduces to the visible energy range (**Figure 1*c*, subpanel *i***) and coincides with the photon energy of the excitation. A similar observation has been made for CO_2 chemisorption on Ag (49). Furthermore, the LUMO-derived MOs have negligible overlap with the metal states, which prolongs the lifetime of the adsorbate photoexcited state. Visible-light excitation causes a direct electronic excitation from the HOMO-derived MO, that is, the nonbonding lone-pair type orbitals on the S atoms (n_S), to the LUMO-derived MO, that is, the AB orbital localized on the S–S bond (σ^*_{SS}), which facilitates the dissociation of the S–S bond (**Figure 1*c*, subpanel *ii***). This role of direct electronic excitations was validated by the observed excitation wavelength dependence of the dissociation yield.

4.2. Adsorbate-Specific Photoactivation and Photodesorption

The strong electronic hybridization present in a metal–adsorbate system can be exploited for activation and desorption of a specific adsorbate by light excitation. Christopher and coworkers (83) demonstrated such adsorbate specificity and harnessed it for the preferential oxidation of CO in an H_2-rich stream on small Pt NPs supported on α-Al_2O_3. Under their reaction conditions, CO oxidation by O_2 is rate-limited by the desorption of adsorbed CO from the Pt surface, whereas H_2 oxidation by O_2 is rate-limited by the desorption of adsorbed O. The researchers showed that, compared to a Pt–O bond, a Pt–CO bond can be selectively photoactivated (83), which triggers the selective desorption of CO, leading to its more selective oxidation as compared to H_2.

The mechanism underpinning this phenomenon is as follows (**Figure 1*d*, subpanel *i***). Normally, localized HOMO-LUMO excitation of CO occurs at ~5 eV. However, the strong chemisorption of CO on Pt(111) results in the hybridization of the surface states of the Pt surface and localized orbitals of CO. Pt–CO AB orbitals of largely molecular character are formed by donation of electron density from CO 5σ states to Pt $6sp$ states. Pt–CO B orbitals of predominantly metal character are formed by the back-donation of electron density from Pt $5d$ states to CO $2\pi^*$ states. The optical gap between the B and AB orbitals is resonant with a 470-nm (2.75-eV) excitation. Irradiation of the Pt NPs by 470-nm light (**Figure 1*d***) induces the direct excitation of an electron into the Pt–CO AB states, thereby weakening the Pt–CO bond and facilitating desorption of CO. As a result, under light excitation of 2.3-nm α-Al_2O_3-supported Pt NPs, CO is oxidized more efficiently than H_2, which is seen from the higher quantum yield of the CO oxidation as compared to that of H_2 oxidation (**Figure 1*d*, subpanel *ii***). The selectivity of CO oxidation peaks at an excitation wavelength of ~470 nm. The selective activation of the Pt–CO bond and preferential CO oxidation is unique for small sub-5-nm Pt NPs that have a larger fraction of surface atoms, which makes electronic excitations in surface adsorbates more likely (**Figure 1*d*, subpanel *ii***).

4.3. Light-Driven Multielectron Redox Chemistry and Bond Formation

The examples described thus far have involved the transient transfer of photogenerated electrons from the plasmonic NP to an adsorbate. Yu & Jain (19, 47, 86) and Jain and coworkers (48, 50, 84, 85) have shown that electron–hole pairs generated by the visible-light excitation of Au NPs can be irreversibly transferred to charge acceptors and harvested for redox and bond formation reactions. These are cases in which the charge transfer forms a stable or long-lived ionic or radical species, which then desorbs from the NP surface, and a redox reaction ensues. The central strategy involves the use of a hole acceptor that is easily oxidized, such as an alcohol. Holes generated in the *sp*- and *d*-bands of Au NPs by visible-light excitation are transferred to the alcohol (ROH). ROH gets oxidized to form an H^+, which is released into solution, and a metastable alkoxy intermediate ($RO^\bullet$), which undergoes further oxidation. In this scenario, the hole transfer becomes irreversible. The photogenerated electrons accumulate in *sp*-band states above the Fermi level in the Au NP, resulting in a raised quasi-Fermi level (E_F') under continuous light excitation. The photocharged NP acts as a source of high-potential electrons, which can be irreversibly captured by electron acceptors, leading to reduction reactions. The visible-light-driven reduction of CO_2, which is kinetically challenging, was achieved by this mechanism (19, 29, 46, 47, 49, 50). CO_2 has a deep-UV range HOMO–LUMO gap that cannot be photochemically activated directly with visible light. However, CO_2 can be activated by the visible-light excitation of Au NPs in the presence of a hole scavenger (**Figure 2*a***). Electrons with a high enough potential transfer to the LUMO of adsorbed CO_2, generating the reduction intermediate, $CO_2^{\bullet-}$, the formation of which is the rate-determining step (RDS) in the reduction of CO_2. The $CO_2^{\bullet-}$ captures additional electrons and H^+ generated by light excitation and is transformed to CH_4, which was found to be the major product under 488-nm and 532-nm excitation of the Au NPs. However, at the higher photon energy, that is, 488-nm excitation, and higher light intensities, C_2H_6 was produced in addition to CH_4 (50). The formation of a C_2 product can be attributed to the feasibility of two electron transfers occurring simultaneously to two adsorbed CO_2 molecules at higher photon fluxes. The simultaneous generation and dimerization of two $CO_2^{\bullet-}$ entities result in the formation of a C_2 intermediate that is transformed to C_2H_6 by further electron and proton transfer steps (**Figure 2*b***). The selectivity of the C_2 product versus the C_1 product was higher at higher light intensities and/or photon energies. This study presents a fine example of the use of light-excitation attributes (photon energy and intensity) for tuning product selectivity (86).

The multielectron, multiproton reduction of CO_2 by H_2O was also accomplished without the use of a hole scavenger by using an imidazolium salt. The imidazolium salt, or its carbene derivative, is thought to complex with CO_2 and preconfigure it for acceptance of a photogenerated electron (19, 47). In this case, the C_1–C_3 hydrocarbons were produced by the electron-mediated reduction of CO_2. The photogenerated holes are captured on a slower timescale by water, H_2O, which is oxidized to hydrogen peroxide, H_2O_2. The overall redox reaction in the absence of the alcohol hole scavenger is thought to be endergonic due to the large potential required for H_2O oxidation. The free energy required for this photosynthetic reaction is sourced from the chemical potential of electron–hole pairs produced by light excitation.

4.4. Light-Induced Suppression of Undesired Pathways

To achieve selectivity in heterogeneous catalysis, not only must the desired reaction be promoted but undesirable alternative reactions must also be suppressed. In a recent study of electrocatalytic O_2 reduction on Ag–Pt nanocages, visible-light excitation of LSPRs was shown to suppress the formation of an undesired product, H_2O_2—which is the primary product under dark conditions—and instead favor H_2O production (87). Hot electrons formed in Ag by photoexcitation may be

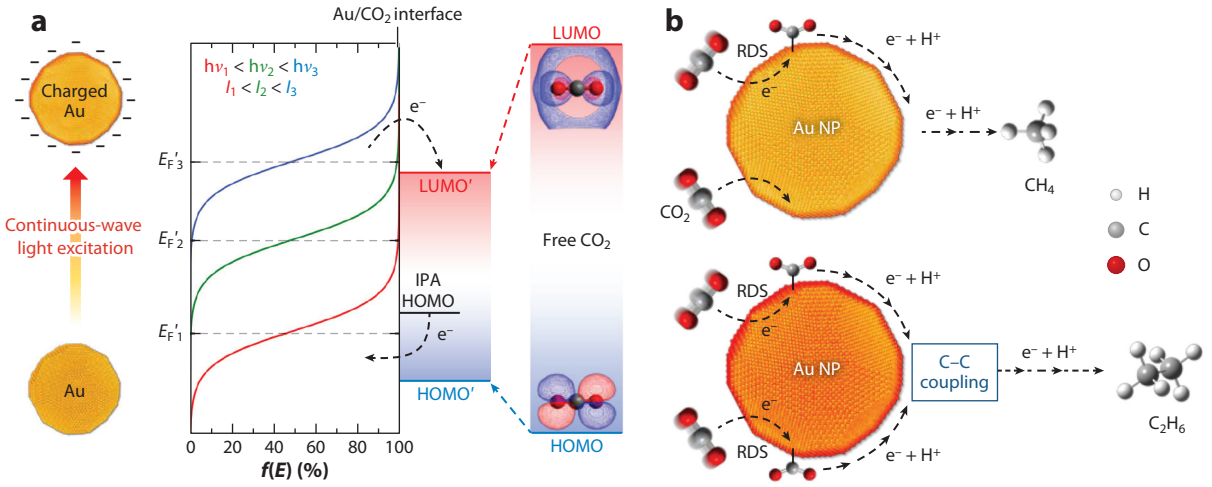

Figure 2

The light-excitation-mediated multielectron reduction of CO_2 and C–C coupling to form hydrocarbons. (*a*) The mechanism of harvesting of electrons and holes from Au NPs under visible-light excitation. When a CO_2 molecule adsorbs onto an Au NP surface, (*right*) an electronic admixture with a smaller HOMO–LUMO gap is formed. Under continuous visible-light excitation of an Au NP in the presence of a hole scavenger such as IPA, holes are annihilated by the injection of electrons from the HOMO of IPA. (*Left*) Due to the faster consumption of holes than of electrons, the Au NP becomes cathodically charged, and (*middle*) has a raised Fermi level (E_F'). E_F' corresponds to the energy at the 50% point in the depicted plot of the percent probability of a state being unoccupied, *f*, as a function of the energy of the state, *E*. The high-potential electrons are injected from the Au NP into the LUMO of the Au–CO_2 admixture. The rate of electron injection depends on the quasi-Fermi level, which is determined by the light-excitation attributes excitation photon energy (hν) and intensity (*I*). (*b*) Schematic of the photoreduction of CO_2 to CH_4 and C_2H_6 on an Au NP under visible-light excitation. (*Top*) Under typical conditions, $CO_2^{\bullet-}$ is formed by the transfer of a photogenerated electron to adsorbed CO_2. Following this RDS, $CO_2^{\bullet-}$ captures multiple electrons and H^+ formed by light excitation, resulting in the formation of CH_4. (*Bottom*) At higher excitation photon energy and/or higher photon flux conditions, the simultaneous generation and dimerization of two $CO_2^{\bullet-}$ entities is possible. The C–C coupling forms a C_2 intermediate, which captures multiple electrons and H^+ to produce C_2H_6. Abbreviations: IPA, isopropyl alcohol; HOMO, highest-occupied molecular orbital; LUMO, lowest-unoccupied molecular orbital; NP, nanoparticle; RDS, rate-determining step. Figure adapted with permission from Reference 50; copyright 2018 American Chemical Society.

transferred to the 5*d* states of Pt, likely by an indirect mechanism (**Figure 3*a*, subpanel *i***). The electron transfer decreases the concentration of *d*-band vacancies on Pt, which is thought to cause an increase in the heterogeneity of charge on the Pt surface, the site of electrocatalytic activity. This effect is proposed to favor O_2 adsorption on Pt. In addition, photogenerated hot electrons transiently have sufficient energy to populate the O_2 AB orbital, which weakens the O–O bond and triggers its cleavage. This favors the formation of H_2O over H_2O_2 (**Figure 3*a*, subpanel *ii***). In the absence of light excitation, the O–O bond is not weakened; instead the dissociation of the O–Pt bond is favored, which results in the reduction of O_2 to undesired peroxide ions, HO_2^- (**Figure 3*a*, subpanel *ii***). Thus, light excitation of a plasmonic nanostructure-based electrocatalyst achieves desirable chemical selectivity by activating a specific chemical bond and suppressing the formation of an undesired intermediate.

4.5. Light-Induced Promotion of Desired Reactions and Suppression of Undesired Competing Reactions

The degree of hot electron–mediated activation and its consequences vary from one adsorbate to another depending on the electronic interaction of the adsorbate with the metal surface.

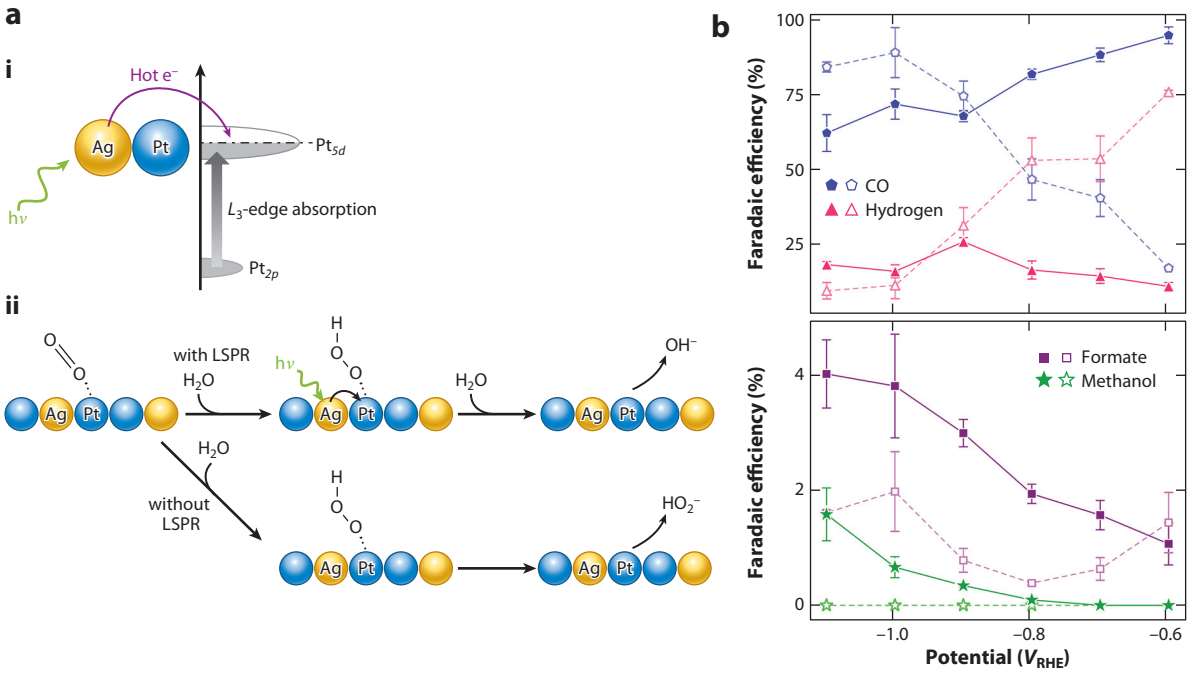

Figure 3

Light-induced suppression of undesired intermediates and competing side reactions mediated by hot electron transfer. (*a*) On Ag–Pt nanostructures, the electrocatalytic reduction of O_2 to H_2O_2 is favored in the dark, whereas under light excitation, H_2O is the major reduction product. The schematic illustrations show the mechanism of this effect. (*i*) Light illumination (hν) excites LSPRs in Ag, the damping of which generates hot electrons (e^-), which are transferred to the 5*d* states of Pt. The decrease in the concentration of vacancies in the 5*d*-band was verified by L_3-edge absorption measurements. (*ii*) The resulting increase in charge heterogeneity on the Pt surface favors O_2 adsorption. The transient population of unoccupied orbitals of adsorbed O_2 by hot electrons triggers O–O bond cleavage. As a result, H_2O formation is favored over H_2O_2 under LSPR excitation. In the dark, because this pathway is not accessible, O–Pt bond dissociation and, consequently, the formation of the peroxide ion, HO_2^-, are favored. Panel *a* adapted with permission from Reference 87; copyright 2017 American Chemical Society. (*b*) Tuning of product selectivity in electrocatalytic CO_2 reduction by light excitation of nanostructured Ag cathodes. Plots of the Faradaic efficiencies of products (*top*, CO and H_2; *bottom*, formate and methanol) generated on nanostructured Ag cathodes as a function of applied potential versus the RHE under 365-nm light excitation of an intensity of 170 mW/cm^2 (*filled symbols*, *solid lines*) and under dark conditions (*open symbols*, *dashed lines*). Light excitation enhances CO_2 reduction to CO and simultaneously suppresses H_2 generation at low cathodic potentials. At high cathodic potentials, formate production is promoted by light excitation; methanol is formed exclusively under light excitation. Panel *b* adapted with permission from Reference 88; copyright 2019 American Chemical Society. Abbreviations: LSPR, localized surface plasmon resonance; RHE, relative hydrogen electrode.

Photoactivation may promote the further reaction of one adsorbed intermediate while retarding that of another. This effect can influence product selectivity, as shown by McCloskey and coworkers (88) in electrocatalytic CO_2 reduction on a nanostructured Ag cathode. At low cathodic potentials, illumination of the plasmonic cathode by 365-nm light of an intensity of 170 mW/cm^2 suppressed the hydrogen evolution—which competes with CO_2 reduction—and promoted the production of CO (**Figure 3*b***). At higher cathodic potentials, the production of formate and methanol was favored under light excitation (**Figure 3*b***). The Faradaic efficiencies of the CO and formate were boosted by light excitation. Most notably, methanol was produced only under light excitation.

The observed selectivity can be explained by the hot electron–mediated activation of adsorbates resulting in different outcomes depending on the adsorbate. Hot electrons generated by light

excitation transiently populate the unoccupied states of the electrocatalyst–adsorbate complex in which the adsorbate is an intermediate in the CO_2 reduction pathway. The generated TNI relaxes and leaves the adsorbate in a vibrationally excited state. This effect may enhance the reactivity of the intermediates in the CO_2 reduction. The applied potential modulates the surface availabilities of specific intermediates involved in the formation of CO, formate, or methanol. In parallel with this photoenhancement, there is also a suppression effect of light excitation. The transient hot electron occupation of energetically accessible electronic states of adsorbed H^+, the intermediate in the H_2 evolution reaction, favors the desorption of H^+ from the electrocatalyst surface. As a result, the electrocatalytic reduction of H^+ becomes less likely at low cathodic potentials, and H_2 formation is suppressed.

4.6. Light-Induced Lowering of the Activation Barrier

In a situation in which several chemical pathways compete, a reduction in the activation energy of formation of a critical intermediate can have a dramatic effect: The associated pathway becomes favored over others, and the product of that pathway becomes selective. Light-induced lowering of the reaction barrier (89, 90) has been observed to be the operative mechanism in photoenhanced ferricyanide reduction (84), CO_2 hydrogenation (91), and NH_3 decomposition (92) on transition metal NPs. These specific examples are elaborated next.

4.6.1. A light-induced increase in Fermi level lowers the apparent barrier for reduction. A systematic kinetic study of the visible-light-excitation-driven reduction of ferricyanide on Au NPs has shown that the apparent activation barrier of the reduction reaction is lowered by light excitation (84). In fact, this effect is responsible for the enhanced rate of ferricyanide reduction under light excitation relative to that in dark conditions. The higher the light intensity is, the lower the apparent barrier is, until this lowering effect plateaus at high intensities. The mechanism for barrier lowering is thought to be as follows. Holes in the *d*-band generated in the Au NPs by visible-light excitation are highly energetic; therefore, the holes are removed by a hole acceptor at a much more rapid rate than are electrons. Hence, under steady-state conditions, there is an excess of electrons on the NP, which accumulate in the *sp* states above the dark Fermi level, resulting in a raised quasi-Fermi level, as explained in Section 4.3. Electrons sourced for ferricyanide reduction from such a charged NP are at a higher potential than are those from an uncharged NP. As a consequence, the activation barrier for the electron-mediated reduction reaction on the NP surface is effectively lower under light excitation as compared to that in the dark. The higher the intensity is, the higher the quasi-Fermi level (up to some limit) is and, consequently, the lower the activation barrier.

4.6.2. Adsorbate-specific activation by hot electrons reduces the activation barriers for desired pathways. Liu, Everitt, and coworkers (91) found that CO_2 hydrogenation on Al_2O_3-supported Rh nanocubes favors CH_4 formation under light excitation, which is otherwise kinetically hindered compared to CO production. UV light with a photon energy of 3.4 eV or blue light with a photon energy of 2.7 eV was used, both of which overlap with the broad UV-region-centered LSPR absorption of Rh nanocubes. The selectivity to CH_4 versus CO was >90% under UV light excitation, much higher than that under dark conditions (**Figure 4*a***). This modulation in the reaction selectivity was accompanied by a decrease in the apparent activation energy of CH_4 formation from ~79 kJ/mol in the dark, that is, thermocatalysis, to ~50 kJ/mol under light excitation. This effect was attributed to hot electrons generated by light excitation.

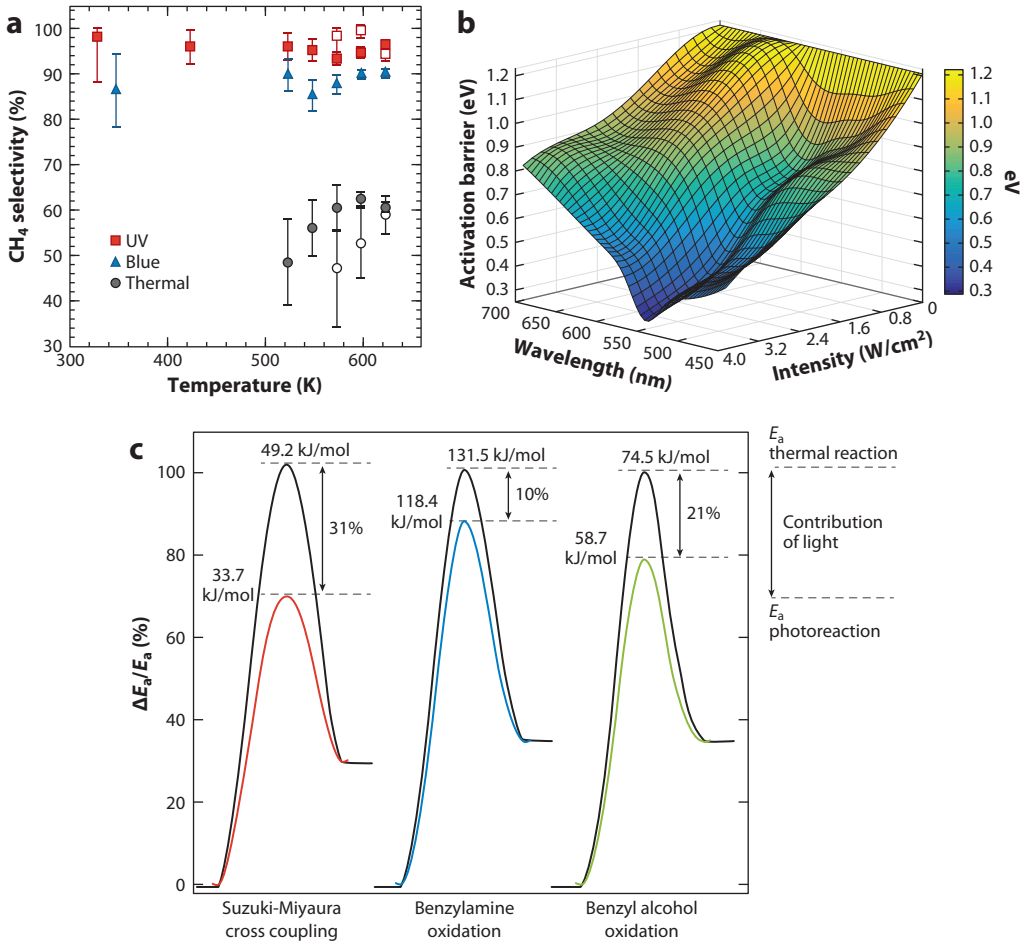

Figure 4

Light-induced lowering of the activation barrier in CO_2 hydrogenation on Al_2O_3-supported Rh nanocubes. (*a*) CH_4 selectivity as a function of temperature observed under three different conditions: excitation by UV light of a photon energy of 3.4 eV and an intensity of 3 W/cm^2; excitation by blue light of a photon energy of 2.7 eV and an intensity of 2.4 W/cm^2; and in the dark, that is, thermal catalytic conditions. At all temperatures, the reaction produced CH_4 with high selectivity under light excitation, whereas in the dark, the selectivity of CH_4 production versus CO production was lower. This effect was accompanied by a light-induced reduction of the activation barrier for the CH_4 formation pathway. Panel *a* adapted with permission from Reference 91; copyright 2017 Springer Nature. (*b*) NH_3 decomposition on Cu nanoparticles with a Cu–Ru surface alloy. This 3D plot shows the apparent activation barrier height of NH_3 decomposition measured under light excitation as a function of the excitation wavelength and light intensity. The measured activation barrier is lower under light excitation as compared to that in the dark (0 W/cm^2 line); the higher the intensity is, the greater the degree of lowering is. Panel *b* adapted from Reference 92 with permission from the American Association for the Advancement of Science. (*c*) In the visible-light-assisted catalysis of organic synthesis reactions, including the Suzuki-Miyaura cross coupling, the oxidative coupling of benzylamine, and benzyl alcohol oxidation, on Au–Pd alloy plasmonic–catalytic nanostructures, the apparent activation barrier height, E_a, is observed to be lower under photoexcitation than is that in a thermal reaction in the dark. Panel *c* adapted with permission from Reference 94; copyright 2013 American Chemical Society.

On an Rh surface, the CO* adsorbate formed from CO_2 dissociation can either desorb from the surface and form CO or undergo further hydrogenation to form CHO*. The CH–O bond of the CHO* intermediate can be cleaved and hydrogenated further to form CH_4. CO desorption is the RDS for CO production, whereas CH–O bond cleavage is the RDS for CH_4 production.

The competition between CO desorption and CH–O bond cleavage dictates the product selectivity. In thermally catalyzed CO_2 hydrogenation, there is no special preference for the thermal activation of the CH–O bond as compared to that of the Rh–CO bond. Therefore, no preference is observed for the formation of CH_4 as compared to that of CO. On the contrary, under photoexcitation, the CH–O bond is selectively activated, which results in near-exclusive production of CH_4. UV- or blue-light excitation of the Rh nanocubes generates hot electrons that occupy states above the Fermi level. High-energy hot electrons generated by UV-light excitation align with the AB orbitals of CHO*, which results in a high probability of their transfer to the C–O π^* AB orbital of CHO*. The transient occupation of hot electrons weakens the C–O bond and promotes the CH_4 formation pathway, which is manifested in a reduced activation energy for this pathway. The Rh–C AB orbital of the CO* adsorbate lies at a much lower energy and is therefore less likely to accept hot electrons. Due to the low likelihood of Rh–C activation, CO formation is therefore inhibited.

4.6.3. The light-induced desorption of adsorbate reduces the activation barriers of overall reactions. In another study, Halas and coworkers (92) investigated the effects of light excitation on the reaction kinetics and apparent activation barrier (E_a) for NH_3 decomposition on nanostructures consisting of a plasmonic antenna Cu NP with a catalytically active Cu–Ru surface alloy. The measured E_a was ~1.21 eV in the dark, but it decreased to ~0.35 eV under illumination with light of an intensity of 3.2 W/cm^2 and a wavelength of 550 nm, which overlaps with the LSPR band of the Cu–Ru nanostructures. The measured E_a decreased further with an increase in the light intensity (**Figure 4*b***), similar to what was observed by Jain and coworkers (84). The observed intensity-dependent decrease in E_a and increase in the reaction order and rate under light illumination were attributed to an effect of hot carriers on the energy landscape of NH_3 decomposition on the Cu–Ru surface. The overall apparent activation energy of the NH_3 decomposition reaction ($E_{a,\,reaction}$) is a function of the activation barriers of the RDSs involved in the reaction ($E_{a,\,RDS}$), the enthalpy of the formation of species involved in the RDS, and the energy required to remove poisoning reaction intermediates from active sites ($E_{a,\,desorption}$). Associative desorption of N_2 and N–H bond scission are the two RDSs of NH_3 decomposition on an Ru surface. The hot carriers formed in the Cu NPs by light excitation are thought to activate the adsorbate, N_{ads}, on the Cu–Ru surface. N_{ads} can be activated by either a resonant hot electron transfer or hot electron–mediated vibrational excitation. The transient transfer of hot electrons from the Cu NP to resonant unoccupied acceptor levels of the Ru–N surface species activates the Ru–N bond. Evolution of the activated Ru–N species along the excited-state PES, which has a lower dissociation barrier than the ground-state PES, triggers N_{ads} removal. Another alternative is the hot electron–mediated vibrational excitation of N_{ads} by inelastic electron–vibrational dipole scattering.

Vibrational energy accumulated from multiple vibrational excitations in the ground state can help N_{ads} overcome the activation barrier for desorption. These processes enhance associative N_2 desorption and consequently lead to a reduction in both $E_{a,\,RDS}$ and $E_{a,\,reaction}$. In addition, hot electrons may promote the desorption of poisoning adsorbates from active sites, a synergistic effect that further lowers $E_{a,\,reaction}$. The higher the light intensity is, the higher the likelihood of hot electron–activated processes is and, consequently, the lower the $E_{a,\,reaction}$.

A photoinduced reduction in the activation energy has also been observed in cross-coupling reactions (**Figure 4*c***), including the Suzuki-Miyaura, Sonogashira, Hiyama, Stille, Buchwald-Hartwig, and Ullmann reactions catalyzed by alloy or bimetallic, that is, plasmonic–catalytic, nanostructures (11, 90, 93, 94, 95). Light excitation is thought to enhance charge heterogeneity on the surface of the catalytic metal, favoring reactant adsorption, which is manifested as a reduction in the apparent activation energy (94).

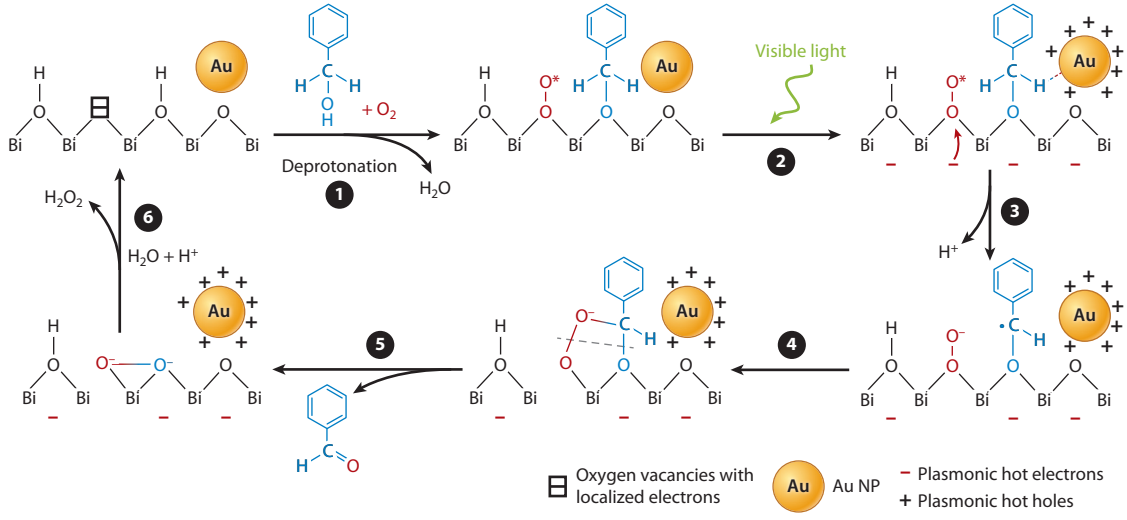

Figure 5

Light-induced surface-radical generation for selective oxidation. Schematic illustration of the proposed mechanistic steps (❶–❻) in the unusual light-driven oxidation of benzyl alcohol (shown in blue) by O_2 (shown in red) on Au nanoparticles (NPs) supported on BiOCl bearing oxygen vacancies. Figure adapted with permission from Reference 96; copyright 2017 American Chemical Society.

4.7. Light-Induced Surface-Radical Generation for Selective Oxidation Reactions

Light excitation of metal NPs can generate free radicals on the catalyst surface, which can then be used for selective oxidation. As an example, Wang and coworkers (96) observed a new reaction pathway (**Figure 5**) when benzyl alcohol oxidation was performed with O_2 in the presence of Au NPs supported on BiOCl bearing oxygen vacancies (OVs) and white-light irradiation. The presence of this new pathway was revealed by their observation that 66% of O atoms in the product benzaldehyde originated from O_2 instead of from the reactant benzyl alcohol. Such O-atom transfer is atypical for benzyl alcohol oxidation and was not observed in the absence of Au NPs (97). The unusual pathway was attributed to the synergistic action of electrons and holes photogenerated in the Au NPs by the excitation of LSPRs. The following light-induced reaction mechanism was proposed (**Figure 5**). O_2 and benzyl alcohol adsorb at OVs on BiOCl. Photogenerated electrons transfer from the Au NPs to O_2 adsorbed at OVs to form $O_2^{\bullet -}$. Concomitantly, photogenerated holes on the Au NP trigger a mild oxidizing action, forming a carbon-centered free radical from benzyl alcohol. $O_2^{\bullet -}$ and the carbon-centered radical then undergo a concerted ring addition on the BiOCl surface to form benzaldehyde with high selectivity and a high prevalence of O atoms from O_2.

4.8. Light-Induced Redox Switching of Catalysts

Light excitation of plasmonic NPs can be exploited not only for activating adsorbates but also for switching the NP surface into a catalytically active state. Cu is active toward propylene epoxidation; in its metallic state, Cu exhibits a high selectivity for the desirable propylene epoxide product. However, under realistic reaction conditions for propylene oxidation, the Cu surface becomes oxidized, which deteriorates its chemical selectivity. Linic and coworkers (4) used plasmonic excitation to overcome this problem. Cu NPs employed for thermocatalytic propylene oxidation

showed a low selectivity (20%) for epoxide production due to the oxidation of the NP surfaces in the O_2-rich stream. However, when the reaction was conducted under ~550 mW/cm^2 of broadband visible-light excitation, a selectivity as high as 50% was achieved. This effect was due to the light-induced switching of surface atoms to the Cu(0) oxidation state. Based on additional studies, a mechanism for this photoswitching has been proposed. Visible light excites LSPRs in the Cu NP cores of the surface-oxidized catalyst. Hot electrons formed in the Cu core as a consequence are transiently injected into Cu–O AB states of the surface Cu_2O. The Cu–O bond weakens, facilitating the reduction of surface Cu_2O to Cu(0). Thus, plasmonic excitation offers a handle to switch the oxidation state of a functioning metal NP catalyst, which in this case enabled the recovery of an active form of the catalyst that has high selectivity for a desired product.

4.9. Wavelength-Tunable Light-Assisted Catalysis Using Plasmonic Metal Nanoparticle–Semiconductor Heterostructures

While plasmonic NPs are suitable platforms for exploring and exploiting light-assisted catalysis, heterostructures of plasmonic metal NPs and semiconductors offer some distinct attributes and functions. Wide band-gap semiconductors are commonly employed as photocatalysts, but they suffer from limitations such as poor photostability and limited absorption of the visible fraction of the solar spectrum (98–102). A plasmonic metal–semiconductor NP heterostructure (103–106) can harvest a greater portion of the visible solar spectrum. These heterostructures exhibit interesting photophysics and carrier dynamics. UV-light excitation of the semiconductor band gap generates conduction band (CB) electrons in the semiconductor. Provided the bands of the metal and semiconductor are suitably aligned, the photogenerated electrons can migrate to the metal NP and accumulate there, forming an electron reservoir. Conversely, hot electrons formed by the plasmonic excitation of the metal NP can migrate to the semiconductor CB (107–113). In either case, back-electron transfer may be prevented by the interfacial Schottky barrier, prolonging the lifetimes of the separated charge carriers (114). In such heterostructures, the excitation wavelength determines the direction of electron transfer and hence the surface on which the electron- and hole-mediated reactions take place (115, 116).

Garcia and coworkers (115) found that the product distribution in light-induced CO_2 reduction by H_2O on TiO_2-supported Au–Cu alloy NPs can be tuned by changing the excitation wavelength. Methane was formed with 97% selectivity under visible-light excitation exposure, whereas UV-light excitation produced H_2 alone. This is due to the different electron-transfer mechanisms thought to be operational under the two excitation wavelengths. UV-light excitation excites a band-gap transition in TiO_2, generating electrons in the CB. These electrons migrate to the Au–Cu NPs, where they trigger H^+ reduction. The holes left over in the valence band of the TiO_2 trigger the oxidation of H_2O to O_2. In contrast, visible-light irradiation excites LSPRs in the Au–Cu NPs; hot electrons formed by LSPR damping populate the Cu–O AB orbitals of Cu_2O on the NP surfaces. The Cu–O bonds are weakened as a result, which favors the formation of Cu(0). The freshly formed Cu(0) sites activate and reduce CO_2 selectively to CH_4. A portion of the photogenerated electrons transfers to the CB of TiO_2, where they drive H^+ reduction. The holes left over in the Au–Cu NPs trigger H_2O oxidation. Thus, depending on the excitation wavelength, the plasmonic Au–Cu NPs can act either as electron reservoirs or light harvesters. As a consequence, the product selectivity is influenced by the excitation wavelength.

5. SUMMARY AND OUTLOOK

The use of light to trigger chemical reactions on nanostructured metal catalyst surfaces is now a heavily researched field of study. However, a less-discussed aspect of this field is the ability of light

excitation to unlock reaction pathways and product selectivity that are not accessible through conventional thermal catalysis. In this article, we reviewed salient examples of and elementary mechanisms responsible for the induction of atypical reaction pathways under light excitation of plasmonic metal NPs. At the heart of these phenomena is the generation of excited electron–hole pairs by the damping of LSPRs excited in the plasmonic NP. Photogenerated carriers can activate specific adsorbates, trigger bond dissociation, or irreversibly transfer to charge acceptors, inducing redox transformations. Other phenomena include the carrier-mediated lowering of the activation barrier of a specific pathway and the destabilization or desorption of a specific reaction intermediate. Through one or more of these mechanisms, light excitation can modify the energy landscape available to the reactive species and lead to pathways not otherwise accessible on the ground-state PES. Furthermore, pathways and selectivity can be tuned by variation of the light-excitation attributes including the photon energy and the intensity.

Light-assisted catalysis can be transformational. However, the major bottleneck for efficient photon harvesting and practical utility is the mismatch between the short lifetimes of energetic charge carriers in a metal NP and the long timescales over which surface chemical reactions take place. This key challenge can be overcome by an improved understanding of the physical chemistry of carrier-driven reactions and the engineering of nanostructures customized for ultrafast charge separation in a wide range of environments. Aspects of these mechanistic models, which are based on deductions from photoreaction studies, need further verification by ultrafast spectroscopy.

DISCLOSURE STATEMENT

The authors are not aware of any affiliations, memberships, funding, or financial holdings that might be perceived as affecting the objectivity of this review.

ACKNOWLEDGMENTS

Funding for this work (contributions of D.D., V.M., and P.K.J.) was provided by the Energy & Biosciences Institute (EBI) through the EBI-Shell program. This material is based in part upon work (contributions of A.D.) supported by the National Science Foundation under grant NSF CHE-1455011.

LITERATURE CITED

1. Hagen J. 2015. *Industrial Catalysis: A Practical Approach*. Somerset, UK: Wiley. 3rd ed.
2. Christopher P, Xin H, Linic S. 2011. Visible-light-enhanced catalytic oxidation reactions on plasmonic silver nanostructures. *Nat. Chem.* 3(6):467–72
3. Christopher P, Xin H, Marimuthu A, Linic S. 2012. Singular characteristics and unique chemical bond activation mechanisms of photocatalytic reactions on plasmonic nanostructures. *Nat. Mater.* 11(12):1044–50
4. Marimuthu A, Zhang J, Linic S. 2013. Tuning selectivity in propylene epoxidation by plasmon mediated photo-switching of Cu oxidation state. *Science* 339(6127):1590–93
5. Mubeen S, Lee J, Singh N, Krämer S, Stucky GD, Moskovits M. 2013. An autonomous photosynthetic device in which all charge carriers derive from surface plasmons. *Nat. Nanotechnol.* 8(4):247–51
6. Lee J, Mubeen S, Ji X, Stucky GD, Moskovits M. 2012. Plasmonic photoanodes for solar water splitting with visible light. *Nano Lett.* 12(9):5014–19
7. Mukherjee S, Zhou L, Goodman AM, Large N, Ayala-Orozco C, et al. 2014. Hot-electron-induced dissociation of H_2 on gold nanoparticles supported on SiO_2. *J. Am. Chem. Soc.* 136(1):64–67

8. Mukherjee S, Libisch F, Large N, Neumann O, Brown LV, et al. 2013. Hot electrons do the impossible: plasmon-induced dissociation of H_2 on Au. *Nano Lett.* 13(1):240–47
9. Cui J, Li Y, Liu L, Chen L, Xu J, et al. 2015. Near-infrared plasmonic-enhanced solar energy harvest for highly efficient photocatalytic reactions. *Nano Lett.* 15(10):6295–301
10. Huang X, Li Y, Chen Y, Zhou H, Duan X, Huang Y. 2013. Plasmonic and catalytic AuPd nanowheels for the efficient conversion of light into chemical energy. *Angew. Chem. Int. Ed.* 52(23):6063–67
11. Wang F, Li C, Chen H, Jiang R, Sun L-D, et al. 2013. Plasmonic harvesting of light energy for Suzuki coupling reactions. *J. Am. Chem. Soc.* 135(15):5588–601
12. Frischkorn C. 2008. Ultrafast reaction dynamics of the associative hydrogen desorption from Ru(001). *J. Phys. Condens. Matter* 20(31):313002
13. Frischkorn C, Wolf M. 2006. Femtochemistry at metal surfaces: nonadiabatic reaction dynamics. *Chem. Rev.* 106(10):4207–33
14. Jain PK. 2019. Taking the heat off of plasmonic chemistry. *J. Phys. Chem. C* 123(40):24347–51
15. Low J, Yu J, Jaroniec M, Wageh S, Al-Ghamdi AA. 2017. Heterojunction photocatalysts. *Adv. Mater.* 29(20):1601694
16. Fu J, Jiang K, Qiu X, Yu J, Liu M. 2020. Product selectivity of photocatalytic CO_2 reduction reactions. *Mater. Today* 32:222–43
17. Fujishima A, Honda K. 1972. Electrochemical photolysis of water at a semiconductor electrode. *Nature* 238(5358):37–38
18. Abe R. 2010. Recent progress on photocatalytic and photoelectrochemical water splitting under visible light irradiation. *J. Photochem. Photobiol. C Photochem. Rev.* 11(4):179–209
19. Yu S, Jain PK. 2019. Plasmonic photosynthesis of C_1–C_3 hydrocarbons from carbon dioxide assisted by an ionic liquid. *Nat. Commun.* 10:2022
20. DuChene JS, Tagliabue G, Welch AJ, Cheng W-H, Atwater HA. 2018. Hot hole collection and photoelectrochemical CO_2 reduction with plasmonic Au/p-GaN photocathodes. *Nano Lett.* 18(4):2545–50
21. Yang J, Hao J, Xu S, Wang Q, Dai J, et al. 2019. $InVO_4$/β-$AgVO_3$ nanocomposite as a direct Z-scheme photocatalyst toward efficient and selective visible-light-driven CO_2 reduction. *ACS Appl. Mater. Interfaces* 11(35):32025–37
22. García-García I, Lovell EC, Wong RJ, Barrio VL, Scott J, et al. 2020. Silver-based plasmonic catalysts for carbon dioxide reduction. *ACS Sustain. Chem. Eng.* 8(4):1879–87
23. Zhou L, Martirez JMP, Finzel J, Zhang C, Swearer DF, et al. 2020. Light-driven methane dry reforming with single atomic site antenna-reactor plasmonic photocatalysts. *Nat. Energy* 5:61–70
24. Kale MJ, Avanesian T, Christopher P. 2014. Direct photocatalysis by plasmonic nanostructures. *ACS Catal.* 4(1):116–28
25. Naldoni A, Shalaev VM, Brongersma ML. 2017. Applying plasmonics to a sustainable future. *Science* 356(6341):908–9
26. Wang C, Astruc D. 2014. Nanogold plasmonic photocatalysis for organic synthesis and clean energy conversion. *Chem. Soc. Rev.* 43(20):7188–216
27. Jain PK, Huang X, El-Sayed IH, El-Sayed MA. 2008. Noble metals on the nanoscale: optical and photothermal properties and some applications in imaging, sensing, biology, and medicine. *Acc. Chem. Res.* 41(12):1578–86
28. Bohren CF. 1983. How can a particle absorb more than the light incident on it? *Am. J. Phys.* 51(4):323–27
29. Yu S, Wilson AJ, Kumari G, Zhang X, Jain PK. 2017. Opportunities and challenges of solar-energy-driven carbon dioxide to fuel conversion with plasmonic catalysts. *ACS Energy Lett.* 2(9):2058–70
30. Hartland GV. 2011. Optical studies of dynamics in noble metal nanostructures. *Chem. Rev.* 111(6):3858–87
31. Khurgin JB. 2015. How to deal with the loss in plasmonics and metamaterials. *Nat. Nanotechnol.* 10:2–6
32. Watanabe K, Menzel D, Nilius N, Freund H-J. 2006. Photochemistry on metal nanoparticles. *Chem. Rev.* 106(10):4301–20
33. Manjavacas A, Liu JG, Kulkarni V, Nordlander P. 2014. Plasmon-induced hot carriers in metallic nanoparticles. *ACS Nano* 8(8):7630–38
34. Linic S, Aslam U, Boerigter C, Morabito M. 2015. Photochemical transformations on plasmonic metal nanoparticles. *Nat. Mater.* 14(6):567–76

35. Swearer DF, Zhao H, Zhou L, Zhang C, Robatjazi H, et al. 2016. Heterometallic antenna–reactor complexes for photocatalysis. *PNAS* 113(32):8916–20
36. Linic S, Christopher P, Xin H, Marimuthu A. 2013. Catalytic and photocatalytic transformations on metal nanoparticles with targeted geometric and plasmonic properties. *Acc. Chem. Res.* 46(8):1890–99
37. Giannini V, Fernández-Domínguez AI, Heck SC, Maier SA. 2011. Plasmonic nanoantennas: fundamentals and their use in controlling the radiative properties of nanoemitters. *Chem. Rev.* 111(6):3888–912
38. Shi X, Ueno K, Takabayashi N, Misawa H. 2013. Plasmon-enhanced photocurrent generation and water oxidation with a gold nanoisland-loaded titanium dioxide photoelectrode. *J. Phys. Chem. C* 117(6):2494–99
39. Voisin C, Del Fatti N, Christofilos D, Vallée F. 2001. Ultrafast electron dynamics and optical nonlinearities in metal nanoparticles. *J. Phys. Chem. B* 105(12):2264–80
40. Brown AM, Sundararaman R, Narang P, Goddard WA III, Atwater HA. 2016. Nonradiative plasmon decay and hot carrier dynamics: effects of phonons, surfaces, and geometry. *ACS Nano* 10(1):957–66
41. Sundararaman R, Narang P, Jermyn AS, Goddard WA III, Atwater HA. 2014. Theoretical predictions for hot-carrier generation from surface plasmon decay. *Nat. Commun.* 5:5788
42. Bernardi M, Mustafa J, Neaton JB, Louie SG. 2015. Theory and computation of hot carriers generated by surface plasmon polaritons in noble metals. *Nat. Commun.* 6:7044
43. Jain PK, Lee KS, El-Sayed IH, El-Sayed MA. 2006. Calculated absorption and scattering properties of gold nanoparticles of different size, shape, and composition: applications in biological imaging and biomedicine. *J. Phys. Chem. B* 110(14):7238–48
44. Sönnichsen C, Franzl T, Wilk T, von Plessen G, Feldmann J, et al. 2002. Drastic reduction of plasmon damping in gold nanorods. *Phys. Rev. Lett.* 88(7):077402
45. Link S, El-Sayed MA. 1999. Spectral properties and relaxation dynamics of surface plasmon electronic oscillations in gold and silver nanodots and nanorods. *J. Phys. Chem. B* 103(40):8410–26
46. Yu S, Mohan V, Jain PK. 2020. Using plasmonically generated carriers as redox equivalents. *MRS Bull.* 45(1):43–48
47. Yu S, Jain PK. 2019. Selective branching of plasmonic photosynthesis into hydrocarbon production and hydrogen generation. *ACS Energy Lett.* 4(9):2295–300
48. Kim Y, Smith JG, Jain PK. 2018. Harvesting multiple electron-hole pairs generated through plasmonic excitation of Au nanoparticles. *Nat. Chem.* 10(7):763–69
49. Kumari G, Zhang X, Devasia D, Heo J, Jain PK. 2018. Watching visible light-driven CO_2 reduction on a plasmonic nanoparticle catalyst. *ACS Nano* 12(8):8330–40
50. Yu S, Wilson AJ, Heo J, Jain PK. 2018. Plasmonic control of multi-electron transfer and C–C coupling in visible-light-driven CO_2 reduction on Au nanoparticles. *Nano Lett.* 18(4):2189–94
51. Smith JG, Faucheaux JA, Jain PK. 2015. Plasmon resonances for solar energy harvesting: a mechanistic outlook. *Nano Today* 10(1):67–80
52. Brongersma ML, Halas NJ, Nordlander P. 2015. Plasmon-induced hot carrier science and technology. *Nat. Nanotechnol.* 10:25–34
53. Zhang Y, He S, Guo W, Hu Y, Huang J, et al. 2018. Surface-plasmon-driven hot electron photochemistry. *Chem. Rev.* 118(6):2927–54
54. Cortés E. 2017. Efficiency and bond selectivity in plasmon-induced photochemistry. *Adv. Opt. Mater.* 5(15):1700191
55. Cortés E, Xie W, Cambiasso J, Jermyn AS, Sundararaman R, et al. 2017. Plasmonic hot electron transport drives nano-localized chemistry. *Nat. Commun.* 8:14880
56. Gadzuk JW. 1983. Vibrational excitation in molecule-surface collisions due to temporary negative molecular ion formation. *J. Chem. Phys.* 79(12):6341–48
57. Zhu X-Y. 2002. Electron transfer at molecule-metal interfaces: a two-photon photoemission study. *Annu. Rev. Phys. Chem.* 53:221–47
58. Ageev VN. 1994. Desorption induced by electronic transitions. *Prog. Surf. Sci.* 47(1–2):55–203
59. Jain PK, Qian W, El-Sayed MA. 2006. Ultrafast cooling of photoexcited electrons in gold nanoparticle–thiolated DNA conjugates involves the dissociation of the gold–thiol bond. *J. Am. Chem. Soc.* 128(7):2426–33

60. Misewich JA, Heinz TF, Newns DM. 1992. Desorption induced by multiple electronic transitions. *Phys. Rev. Lett.* 68(25):3737–40
61. Kazuma E, Jung J, Ueba H, Trenary M, Kim Y. 2018. Real-space and real-time observation of a plasmon-induced chemical reaction of a single molecule. *Science* 360(6388):521–26
62. Boerigter C, Aslam U, Linic S. 2016. Mechanism of charge transfer from plasmonic nanostructures to chemically attached materials. *ACS Nano* 10(6):6108–15
63. Christopher P, Moskovits M. 2017. Hot charge carrier transmission from plasmonic nanostructures. *Annu. Rev. Phys. Chem.* 68:379–98
64. Govorov AO, Zhang H, Gun'ko YK. 2013. Theory of photoinjection of hot plasmonic carriers from metal nanostructures into semiconductors and surface molecules. *J. Phys. Chem. C* 117(32):16616–31
65. Boerigter C, Campana R, Morabito M, Linic S. 2016. Evidence and implications of direct charge excitation as the dominant mechanism in plasmon-mediated photocatalysis. *Nat. Commun.* 7:10545
66. Hövel H, Fritz S, Hilger A, Kreibig U, Vollmer M. 1993. Width of cluster plasmon resonances: bulk dielectric functions and chemical interface damping. *Phys. Rev. B* 48(24):18178–88
67. Foerster B, Joplin A, Kaefer K, Celiksoy S, Link S, Sönnichsen C. 2017. Chemical interface damping depends on electrons reaching the surface. *ACS Nano* 11(3):2886–93
68. Douglas-Gallardo OA, Berdakin M, Sánchez CG. 2016. Atomistic insights into chemical interface damping of surface plasmon excitations in silver nanoclusters. *J. Phys. Chem. C* 120(42):24389–99
69. Yang H, Wang Z-H, Zheng Y-Y, He L-Q, Zhan C, et al. 2016. Tunable wavelength enhanced photoelectrochemical cells from surface plasmon resonance. *J. Am. Chem. Soc.* 138(50):16204–7
70. Liu L, Ouyang S, Ye J. 2013. Gold-nanorod-photosensitized titanium dioxide with wide-range visible-light harvesting based on localized surface plasmon resonance. *Angew. Chem. Int. Ed.* 52(26):6689–93
71. Meng X, Liu L, Ouyang S, Xu H, Wang D, et al. 2016. Nanometals for solar-to-chemical energy conversion: from semiconductor-based photocatalysis to plasmon-mediated photocatalysis and photothermocatalysis. *Adv. Mater.* 28(32):6781–803
72. Pu Y-C, Wang G, Chang K-D, Ling Y, Lin Y-K, et al. 2013. Au nanostructure-decorated TiO_2 nanowires exhibiting photoactivity across entire UV-visible region for photoelectrochemical water splitting. *Nano Lett.* 13(8):3817–23
73. Teranishi M, Wada M, Naya S, Tada H. 2016. Size-dependence of the activity of gold nanoparticle-loaded titanium(IV) oxide plasmonic photocatalyst for water oxidation. *Chem. Phys. Chem.* 17(18):2813–17
74. Bastús NG, Comenge J, Puntes V. 2011. Kinetically controlled seeded growth synthesis of citrate-stabilized gold nanoparticles of up to 200 nm: size focusing versus Ostwald ripening. *Langmuir* 27(17):11098–105
75. Zhou M, Zeng C, Chen Y, Zhao S, Sfeir MY, et al. 2016. Evolution from the plasmon to exciton state in ligand-protected atomically precise gold nanoparticles. *Nat. Commun.* 7:13240
76. Wittstock A, Zielasek V, Biener J, Friend CM, Bäumer M. 2010. Nanoporous gold catalysts for selective gas-phase oxidative coupling of methanol at low temperature. *Science* 327(5963):319–22
77. Hammer B, Norskov JK. 1995. Why gold is the noblest of all the metals. *Nature* 376(6537):238–40
78. Kazuma E, Jung J, Ueba H, Trenary M, Kim Y. 2017. Direct pathway to molecular photodissociation on metal surfaces using visible light. *J. Am. Chem. Soc.* 139(8):3115–21
79. Zhou L, Zhang C, McClain MJ, Manjavacas A, Krauter CM, et al. 2016. Aluminum nanocrystals as a plasmonic photocatalyst for hydrogen dissociation. *Nano Lett.* 16(2):1478–84
80. Zhang C, Zhao H, Zhou L, Schlather AE, Dong L, et al. 2016. Al-Pd nanodisk heterodimers as antenna-reactor photocatalysts. *Nano Lett.* 16(10):6677–82
81. Huang Y-F, Zhang M, Zhao L-B, Feng J-M, Wu D-Y, et al. 2014. Activation of oxygen on gold and silver nanoparticles assisted by surface plasmon resonances. *Angew. Chem. Int. Ed.* 53(9):2353–57
82. Zhang X, Kumari G, Heo J, Jain PK. 2018. In situ formation of catalytically active graphene in ethylene photo-epoxidation. *Nat. Commun.* 9:3056
83. Kale MJ, Avanesian T, Xin H, Yan J, Christopher P. 2014. Controlling catalytic selectivity on metal nanoparticles by direct photoexcitation of adsorbate-metal bonds. *Nano Lett.* 14(9):5405–12
84. Kim Y, Dumett Torres D, Jain PK. 2016. Activation energies of plasmonic catalysts. *Nano Lett.* 16(5):3399–407

85. Kim Y, Wilson AJ, Jain PK. 2017. The nature of plasmonically assisted hot-electron transfer in a donor-bridge-acceptor complex. *ACS Catal.* 7(7):4360–65
86. Yu S, Jain PK. 2020. The chemical potential of plasmonic excitations. *Angew. Chem. Int. Ed.* 59(5):2085–88
87. Lin S-C, Hsu C-S, Chiu S-Y, Liao T-Y, Chen HM. 2017. Edgeless Ag–Pt bimetallic nanocages: in situ monitor plasmon-induced suppression of hydrogen peroxide formation. *J. Am. Chem. Soc.* 139(6):2224–33
88. Creel EB, Corson ER, Eichhorn J, Kostecki R, Urban JJ, McCloskey BD. 2019. Directing selectivity of electrochemical carbon dioxide reduction using plasmonics. *ACS Energy Lett.* 4(5):1098–105
89. Wilson AJ, Mohan V, Jain PK. 2019. Mechanistic understanding of plasmon-enhanced electrochemistry. *J. Phys. Chem. C* 123(48):29360–69
90. Xiao Q, Sarina S, Bo A, Jia J, Liu H, et al. 2014. Visible light-driven cross-coupling reactions at lower temperatures using a photocatalyst of palladium and gold alloy nanoparticles. *ACS Catal.* 4(6):1725–34
91. Zhang X, Li X, Zhang D, Su NQ, Yang W, et al. 2017. Product selectivity in plasmonic photocatalysis for carbon dioxide hydrogenation. *Nat. Commun.* 8:14542
92. Zhou L, Swearer DF, Zhang C, Robatjazi H, Zhao H, et al. 2018. Quantifying hot carrier and thermal contributions in plasmonic photocatalysis. *Science* 362(6410):69–72
93. Gellé A, Jin T, de la Garza L, Price GD, Besteiro LV, Moores A. 2020. Applications of plasmon-enhanced nanocatalysis to organic transformations. *Chem. Rev.* 120(2):986–1041
94. Sarina S, Zhu H, Jaatinen E, Xiao Q, Liu H, et al. 2013. Enhancing catalytic performance of palladium in gold and palladium alloy nanoparticles for organic synthesis reactions through visible light irradiation at ambient temperatures. *J. Am. Chem. Soc.* 135(15):5793–801
95. Aslam U, Chavez S, Linic S. 2017. Controlling energy flow in multimetallic nanostructures for plasmonic catalysis. *Nat. Nanotechnol.* 12(10):1000–5
96. Li H, Qin F, Yang Z, Cui X, Wang J, Zhang L. 2017. New reaction pathway induced by plasmon for selective benzyl alcohol oxidation on BiOCl possessing oxygen vacancies. *J. Am. Chem. Soc.* 139(9):3513–21
97. Hallett-Tapley GL, Silvero MJ, González-Béjar M, Grenier M, Netto-Ferreira JC, Scaiano JC. 2011. Plasmon-mediated catalytic oxidation of *sec*-phenethyl and benzyl alcohols. *J. Phys. Chem. C* 115(21):10784–90
98. Fox MA, Dulay MT. 1993. Heterogeneous photocatalysis. *Chem. Rev.* 93(1):341–57
99. Linsebigler AL, Lu G, Yates JT. 1995. Photocatalysis on TiO_2 surfaces: principles, mechanisms, and selected results. *Chem. Rev.* 95(3):735–58
100. Le Formal F, Pendlebury SR, Cornuz M, Tilley SD, Grätzel M, Durrant JR. 2014. Back electron-hole recombination in hematite photoanodes for water splitting. *J. Am. Chem. Soc.* 136(6):2564–74
101. Cowan AJ, Tang J, Leng W, Durrant JR, Klug DR. 2010. Water splitting by nanocrystalline TiO_2 in a complete photoelectrochemical cell exhibits efficiencies limited by charge recombination. *J. Phys. Chem. C* 114(9):4208–14
102. Kudo A, Miseki Y. 2008. Heterogeneous photocatalyst materials for water splitting. *Chem. Soc. Rev.* 38:253–78
103. Murdoch M, Waterhouse GIN, Nadeem MA, Metson JB, Keane MA, et al. 2011. The effect of gold loading and particle size on photocatalytic hydrogen production from ethanol over Au/TiO_2 nanoparticles. *Nat. Chem.* 3(6):489–92
104. Wang S, Gao Y, Miao S, Liu T, Mu L, et al. 2017. Positioning the water oxidation reaction sites in plasmonic photocatalysts. *J. Am. Chem. Soc.* 139(34):11771–78
105. Huang J, Guo W, Hu Y, Wei WD. 2020. Plasmonic metal–semiconductor heterostructures for hot-electron-driven photochemistry. *MRS Bull.* 45:37–42
106. Shaik F, Peer I, Jain PK, Amirav L. 2018. Plasmon-enhanced multicarrier photocatalysis. *Nano Lett.* 18(7):4370–76
107. Warren SC, Thimsen E. 2012. Plasmonic solar water splitting. *Energy Environ. Sci.* 5:5133–46
108. Cushing SK, Wu N. 2016. Progress and perspectives of plasmon-enhanced solar energy conversion. *J. Phys. Chem. Lett.* 7(4):666–75

109. Knight MW, Sobhani H, Nordlander P, Halas NJ. 2011. Photodetection with active optical antennas. *Science* 332(6030):702–4
110. Qian K, Sweeny BC, Johnston-Peck AC, Niu W, Graham JO, et al. 2014. Surface plasmon-driven water reduction: gold nanoparticle size matters. *J. Am. Chem. Soc.* 136(28):9842–45
111. Tian Y, Tatsuma T. 2005. Mechanisms and applications of plasmon-induced charge separation at TiO_2 films loaded with gold nanoparticles. *J. Am. Chem. Soc.* 127(20):7632–37
112. Wu K, Chen J, McBride JR, Lian T. 2015. Efficient hot-electron transfer by a plasmon-induced interfacial charge-transfer transition. *Science* 349(6248):632–35
113. Furube A, Du L, Hara K, Katoh R, Tachiya M. 2007. Ultrafast plasmon-induced electron transfer from gold nanodots into TiO_2 nanoparticles. *J. Am. Chem. Soc.* 129(48):14852–53
114. DuChene JS, Sweeny BC, Johnston-Peck AC, Su D, Stach EA, Wei WD. 2014. Prolonged hot electron dynamics in plasmonic-metal/semiconductor heterostructures with implications for solar photocatalysis. *Angew. Chem. Int. Ed.* 53(30):7887–91
115. Neaţu Ş, Maciá-Agulló JA, Concepción P, Garcia H. 2014. Gold-copper nanoalloys supported on TiO_2 as photocatalysts for CO_2 reduction by water. *J. Am. Chem. Soc.* 136(45):15969–76
116. Gomes Silva C, Juárez R, Marino T, Molinari R, García H. 2011. Influence of excitation wavelength (UV or visible light) on the photocatalytic activity of titania containing gold nanoparticles for the generation of hydrogen or oxygen from water. *J. Am. Chem. Soc.* 133(3):595–602